Noise sustained propagation: Local versus global noise

M. Löcher,[1,*] N. Chatterjee,[2] F. Marchesoni,[3] W. L. Ditto,[1] and E. R. Hunt[2]
[1]*School of Physics, Georgia Institute of Technology, Atlanta, Georgia 30332-0430*
[2]*Department of Physics and Astronomy, Ohio University, Athens, Ohio 45701*
[3]*Instituto di Fisica della Materia, Universita' di Camerino, I-62032 Camerino, Italy and Department of Physics, University of Michigan, Ann Arbor, Michigan 48109-1120*
(Received 24 November 1999)

We expand on prior results on noise supported signal propagation in arrays of coupled bistable elements. We present and compare experimental and numerical results for kink propagation under the influence of local and global fluctuations. As demonstrated previously for local noise, an optimum range of global noise power exists for which the medium acts as a reliable transmission ''channel.'' We discuss implications for propagation failure in a model of cardiac tissue, and present a general theoretical framework based on discrete kink statistics. Valid for generic bistable chains, the theory captures the essential features observed in our experiments and numerical simulations.

PACS number(s): 05.40.−a, 02.50.−r, 05.45.−a, 87.10.+e

I. INTRODUCTION

Information transfer through nonlinear systems in the presence of fluctuations has been extensively studied in the context of stochastic resonance (SR) [1]. The frontier of this research has shifted toward systems with spatial degrees of freedom over the past few years. While the efforts initially were directed towards enhancing the basic SR effect [2], recent work has demonstrated that noise can also sustain wave propagation [3–5]. In early studies, Jung and Mayer-Kress [3] showed that noise can sustain spiral waves in a caricature model of excitable media. The assisting role of noise for one- and two-dimensional, nonlinear wave propagation was experimentally confirmed by Kádár *et al.* [3] in a chemical medium, and by Löcher *et al.* [4] in an array of coupled electronic resonators. Noise enhanced propagation (NEP) for *periodic* signals was explored by Lindner *et al.* [3] in a chain of coupled, overdamped bistable oscillators. The authors of Ref. [5] furnished evidence of self-organized criticality underlying the creation and propagation of waves by noise in a chemical subexcitable medium. So far, all experiments and simulations on NEP utilized *local and additive* noise. To our knowledge, no comparative studies on the effectiveness of local vs global and additive vs multiplicative noise have been attempted.

In this paper, we experimentally investigate the effectiveness of global noise as compared to local noise for the propagation of a signal in a chain of coupled bistable elements. Expanding on earlier reports [4], the experiments are performed using a 16×16 array of diode resonators driven in the stable period-2 regime. A bias consisting of a second drive at half the main frequency renders one phase more stable, and a phase kink can be made to propagate across the array. For an intermediate value of the coupling resistors and small bias, we observe propagation failure. Adding noise to the drive of each element, either from a single source or from individual sources—corresponding to global and local noise, respectively—greatly increases the chances of successful signal transmission. Digital simulations of NEP in a simple model of cardiac tissue compare favorably with these observations, and allow us to investigate the effects of parameter mismatch between the elements. Finally, we present theoretical insights borrowed from discrete kink statistics which describe the phenomena in reasonable agreement.

II. EXPERIMENTAL RESULTS

The experimental setup consists of 256 coupled diode resonators, of which one element is shown in Fig. 1. The elements are arranged in a 16×16 array with periodic boundary conditions connected along two opposite edges. Each diode resonator works as a bistable element when driven in its period-2 state. We break the phase symmetry by adding to

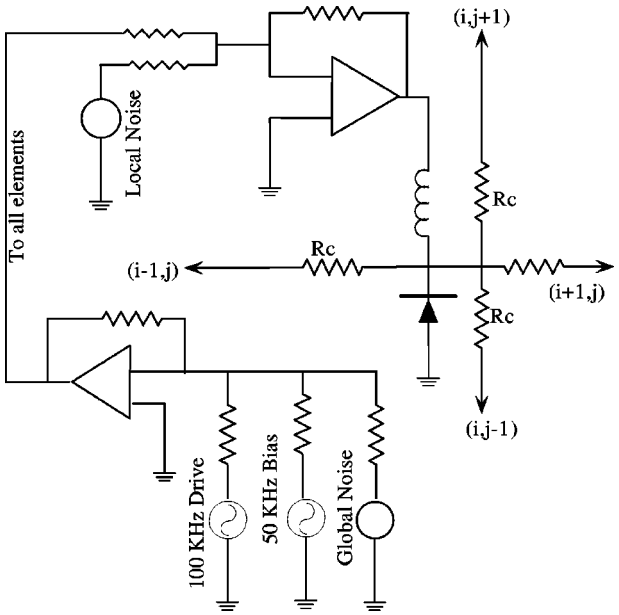

FIG. 1. Experimental circuit arrangement for any node (i,j). We either add noise locally, as shown, or globally by adding one noise source to the main drive. Coupling is provided by the resistors R_C.

*Present address: Siemens Corporate Research, 755 College Rd., Princeton, NJ 08550.

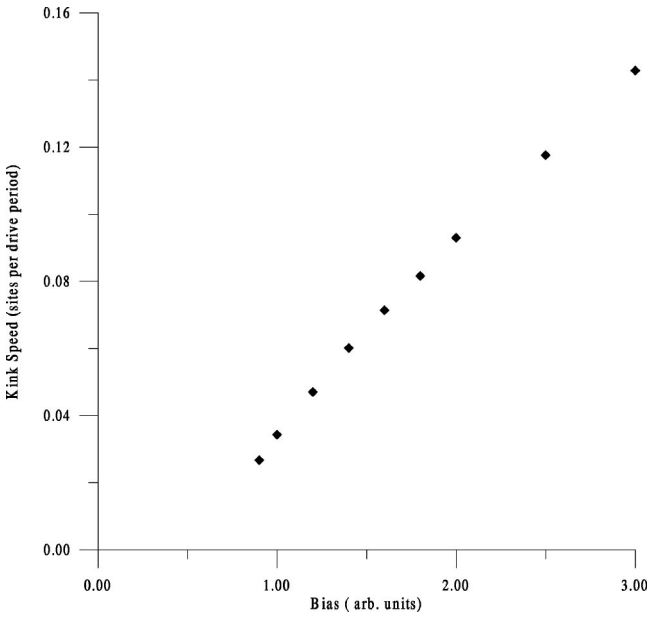

FIG. 2. Kink velocity as a function of the bias for an intermediate value of the coupling resistor R_C. The kink speed shows an approximate linear decrease with bias, down to a cutoff value of approximately 0.9 units.

the drive a second sinusoidal signal at half its frequency. This bias renders one phase more stable. We refer to the less stable phase as the metastable state. By inducing a phase change at one edge of the array, a one-dimensional wave front comprised of phase kinks will travel toward the detector at the other edge. The noise generators were constructed using the shot noise generated by a current through a *pn* junction diode as a source.

It is clear that in the absence of noise, a local phase jump will lead to a ''domino effect'' only if the bias and coupling are strong enough. The energetically lower phase then propagates into the metastable phase in the form of a moving kink. For identical elements, the speed of this moving interface depends on both the coupling strength and the amplitude of the applied bias. If the latter two parameters are chosen to be low enough, kinks in discrete systems will fail to propagate. In the experiment, there is a third factor contributing to kink trapping, namely, heterogeneity of the chain. In our system, the variation of key parameters of the diode resonators and the difference in local noise power is as high as 10%. Arranging the array with periodic boundary conditions in one dimension and preserving the motion of wave fronts in the other dimension, we considerably reduce inhomogenities by effectively averaging over 16 elements.

Figure 2 displays the measured kink velocities in the absence of noise as a function of bias for an intermediate value of the coupling resistors. The velocity decreases approximately linearly with the bias down to a cutoff value of 0.9 units, where it rapidly falls off to zero. We operate the array at a bias of 0.6 units for which the system is not capable of deterministic kink motion.

Our experimental results are given in terms of the arrival-probability curves shown in Fig. 3. The procedure for obtaining these are analogous to those described in Ref. [4]: We reset all resonators to be in the metastable state, and then induce a phase flip at one edge of the array. Any successful kink propagation generates a step function at the detector, which we average over approximately 100 events, resulting in a smooth rise curve (solid lines). In order to quantify transmission degeneration by noise nucleated spurious signals, we repeat the same experiment without inducing a phase flip initially (dashed lines).

The arrival-probability curves for both local and global noise at five different noise strengths are shown in Fig. 3. For local, i.e., independent from site to site, noise, we obtain results analogous to those previously reported [4]. For a local noise background of less than 0.0025 mV^2/Hz [Fig. 3(a)], kinks remained trapped longer than the measurement time of 5000 drive cycles. At 0.0121 mV^2/Hz the signals arrive with a wide distribution of travel times and a slow mean [Fig. 3(b)]. The arrival times become shorter with increasing noise strengths [Figs. 3(c) and 3(d)]. Finally, at 0.0625 mV^2/Hz a substantial number of false starts (dashed lines) corrupt the detection of the original input signal.

We found that the qualitative behavior of the chain under the influence of global noise is similar, but the onset of detectable kink propagation is found at much lower noise strengths. We observe no kink propagation below noise levels of 0.001 mV^2/Hz. Slow and disperse kink motion occurs for noise levels of 0.0025 mV^2/Hz [Fig. 3(a)]. Higher average kink speeds and less fluctuations are recorded for levels of 0.0121 and 0.0256 mV^2/Hz [Figs. 3(b) and 3(c)], while the signal is severely corrupted for values $\geqslant 0.04$ mV^2/Hz [Figs. 3(d) and 3(e)].

Figure 4 compares the velocities of the propagating wave front as a function of the noise strength for both global and local noise. The velocity of the propagating wave front shows an approximate linear increase with increasing noise strength in both cases. Note that the velocity is simply the inverse of the measured arrival times multiplied by the number of sites. It is hence well defined only for low noise levels; in the case of substantial nucleation of additional thermal kinks-antikink pairs this calculated ''velocity'' should be interpreted with caution. Therefore, the data points in Figs. 4 and 7 which correspond to significant noise corruption should be considered as outliers. For the coupling resistors used, the velocity for the global noise case is about 15% greater than that seen for local noise.

Besides the earlier onset in the case of global noise, there are also notable differences in the mechanism that leads to spurious signals. Clearly, for identical elements—unlike spatially uncorrelated noise—global noise cannot induce spurious kinks, which then compete with the deterministic kink due to the signal. The only way of generating a ''false alarm'' at the detector would be to phase flip the entire chain, thus requiring a single large fluctuation. This picture is not fully correct if there are mismatches between the elements, but illustrates the dominant mechanism of creating the signal-masking noise background. Independent noise sources, however, easily spawn spurious kinks, but rarely ever cause a global phase flip of the array. We postulate that the mechanism of noise sustained propagation *per se* is not very different for local and global noise, presuming the kink width is small (i.e., involving a few elements only). The reason for this conjecture is the local nature of the stochastic escape processes that provide for the average effective kink displacement. As long as the spatial correlation length of the

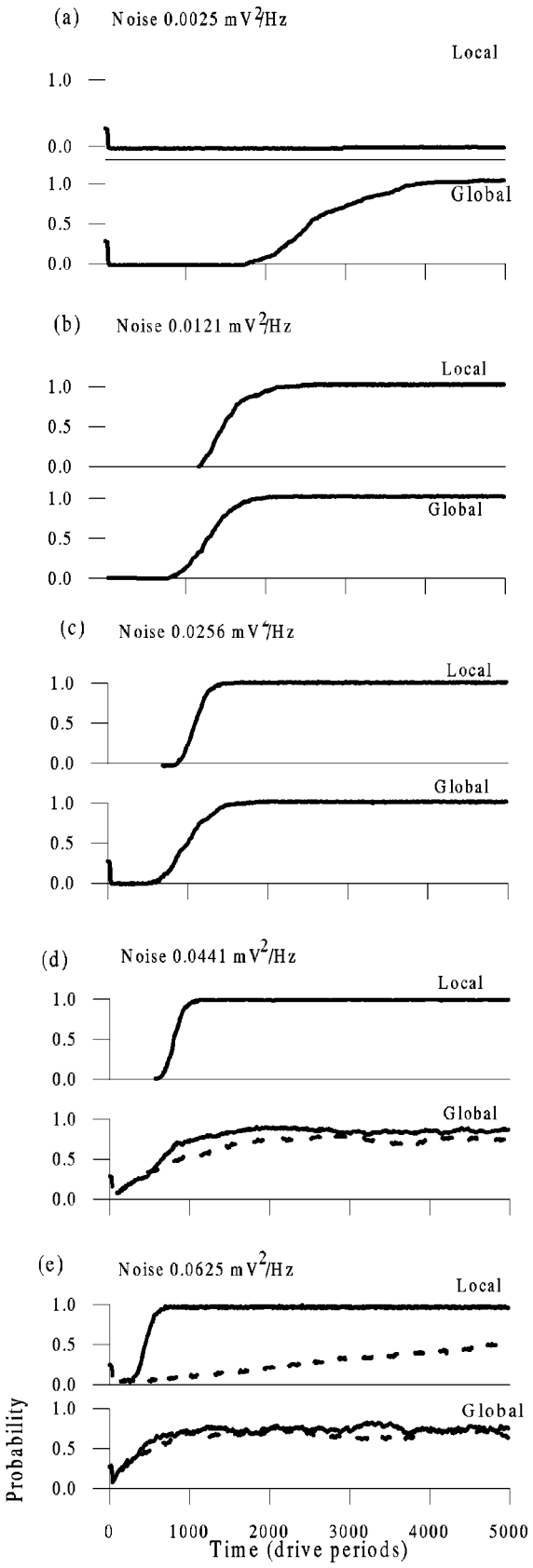

FIG. 3. Arrival probablity of a signal at the end of the chain with (solid line) and without (dashed curves) an induced kink at the beginning, for five local and global noise levels increasing from top to bottom.

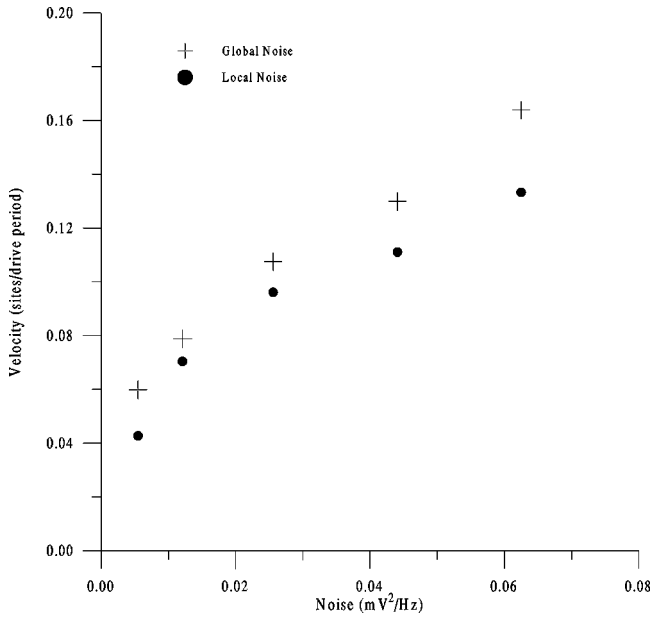

FIG. 4. Experimentally observed average kink velocities as a function of noise strength for both global and local noise. Note that the last (two) data point(s) for local (global) noise are corrupted by noise, and should be interpreted as velocity only with caution.

noise is not substantially smaller than the kink width, the noise induced ''propulsion '' of the kink will be similar for global and local noise. Note that the findings of Kádár *et al.* [3], who briefly addressed the issue of noise correlation lengths, are consistent with this conjecture.

III. SIMULATIONS OF A MODEL OF CARDIAC TISSUE

Propagation failure of signals due to discreteness of the supporting medium was previously observed in theoretical [6] and experimental [7] studies of cardiac tissue. In particular, Keener introduced a modified cable theory, which incorporates the discretizing effects of the so-called *gap junctions* [6]. Gap junctions, characterized by the (relatively high) intercellular resistance r_g, provide the electrical coupling between cardiac cells. Mathematically, the propagation of action potential along cardiac cells is described by various cable theories, which are analogous to wave propagation in one-dimensional conductors (cables). Formally, continuous and discrete models describe the wave propagation by either a partial differential equation or—in the latter case—via coupled ordinary differential equations. *Continuous cable theory* either ignores the effects of the gap junctions or replaces the cytoplasmic resistance with an effective resistance; in either case the electrical resistance is assumed to be spatially homogeneous. Here we focus on the opposite assumption, that gap junctional resistance is much more important than cytoplasmic resistance. We thus neglect the dynamics within a cell and assume that the propagation of the action potential is dominated by the delay caused by the gap junctions [8]. Within the context of this *discrete cable theory*, we can write the current balance as [6]

$$C_m S \frac{d\phi_n}{dt} = \frac{1}{r_g}(\phi_{n+1} - 2\phi_n + \phi_{n-1}) + SI_m(\phi_n), \qquad (1)$$

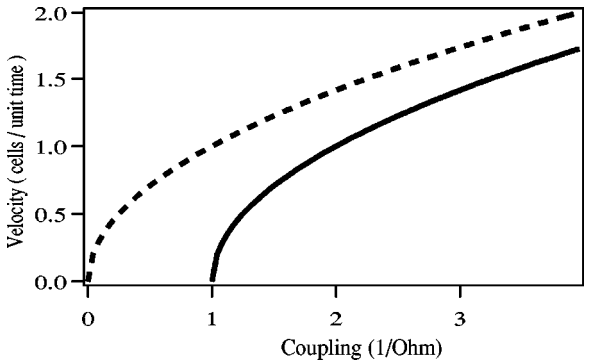

FIG. 5. Kink speed as a function of coupling strength $d=1/r_g$ for the continuous model equation (2) (dashed line) and the discrete model equation (1) (solid line). Note that propagation in the discrete model is impossible for $r_g>r^*$ ($d<d^*=1/r^*$). For this simulation, $C_mS=1$ and $SI_m(\phi)=12\sqrt{3}\phi(1-\phi)(\phi-0.5)+0.5$.

where ϕ_n is the transmembrane potential for the nth cell, S is the surface area of cell membrane, and C_m is the membrane capacitance per unit area of membrane. I_m specifies the inward ionic currents per unit area of the membrane, and is generally postulated to be a function of ϕ_n, having three zeros. For simplicity, we choose a simple cubic polynomial $SI_m(\phi)=12\sqrt{3}\phi(1-\phi)(\phi-0.5)+0.5$ [6]. Note that though similar in appearance, Eq. (1) is *not* simply a discretization of its continuous analog

$$C_mS\frac{\partial\Phi}{\partial t}=\frac{L^2}{r_g}\frac{\partial^2\Phi}{\partial x^2}+SI_m(\phi) \tag{2}$$

(where L is the size of the cardiac cell), but stands in its own right as a spatially discrete nonlinear wave equation. The most important observation is that propagation can fail in model (1) if r_g is sufficiently large, but increasing resistances in Eq. (2) can never lead to propagation failure. Note that r_g depends on the excitability of the tissue.

Figure 5 shows a plot of the numerically determined speed (solid line) of propagation for model (1) as a function of the coupling strength $d=1/r_g$, as well as the analytically obtained kink speed $c=(c_0L/C_mR_m)\sqrt{d}$ (dashed line) for Eq. (2). The reader is referred to Ref. [6] for an explanation of c_0 and R_m. It is evident that propagation is impossible for r_g larger than a certain critical value r^*, which turns out to be a monotonic increasing function of excitability [6].

We have performed digital simulations of the stochastic modification of Eq. (1),

$$\frac{d\phi_n}{dt}=\epsilon(\phi_{n+1}-2\phi_n+\phi_{n-1})+SI_m(\phi_n)[1+\xi_M(t)]+\xi_A(t), \tag{3}$$

using the Euler-Maruyama algorithm [9] with a time step of $dt=0.05$ and a coupling strength $\epsilon=0.07$ (40 elements). $\xi_A(t)$ and $\xi_M(t)$ are additive and multiplicative Gaussian white noise, band limited in practice by the Nyquist frequency $f_N=1/2dt$. We quantify the noise by its dimensionless variance $\sigma^2=2Df_N$, where $2D$ is the height of the one-sided noise spectrum.

Here we only consider the case of purely additive noise, $\xi_M(t)=0$. By following an analogous procedure to that in the experiment, we obtain the probabilities for successful signal transmission as illustrated in Fig. 6. As in the experiment, global noise provides for kink propagation at much lower values of σ^2 than local noise does. Figure 7 compares the velocities of the noise propulsed kink as a function of σ^2 for both global and local noise. The velocity of the propagating wave front shows an approximately parabolic dependence on the noise power in both cases. For the coupling strength employed, global noise leads to speeds about 15% greater than that observed for local noise.

IV. DETECTION CRITERIA

The decision of whether a kink arriving at the last element corresponds to a signal injected at the first site constitutes a simple binary hypothesis-testing problem [10]. We assign the null hypothesis H_0 to ''no signal injected,'' and the opposite for the alternative hypothesis H_1. Denote the according decisions D_i as the judgment that hypothesis H_i was in effect. Clearly, there are two possible errors: A so-called *type I error* occurs when making the decision that H_1 was in effect while the contrary is true. Borrowing notation from radar detection, we refer to this as the probability of *false alarm*, $P_f=P(D_1|H_0)$. On the other hand, if H_1 was in effect to generate the data, and we decide D_0, then we have committed a *type II error*, which in radar is referred to as a *missed detection* [10]. We do that with some probability $P(D_0|H_1)$ which is related to the *probability of detection* $P_d=P(D_1|H_1)$ in an inverse fashion: $P_d=1-P(D_0|H_1)$.

In our experiment, there is no uniquely defined, objectively ''best'' noise level without first defining a decision strategy. Two suitable approaches are (i) the *Neyman-Pearson strategy*, in which the probability of detection P_d is maximized while specifying an upper bound for the false alarm probability P_f; and (ii) *Bayes' rule*, which assigns costs to the various outcomes of the decision process, such as correctly detecting a signal or being ''deceived'' by a spurious kink. The optimum noise level in the latter case would be the one, which minimizes the total average cost.

In communication systems one is usually interested in the total probability of error $P_e=P(D_1|H_0)+P(D_0|H_1)=P_f+1-P_d$. Though in the experimental setup there is no inherent time scale, i.e., the decision when to reset the chain is rather arbitrary, in digital communication applications we would expect information bits to be sent at a constant rate. Hence we choose a reasonable time interval, at the end of which we measure the probabilities of false alarm P_f and missed detection $1-P_d$ as functions of noise power. Then P_f is simply the value of the dashed line in Fig. 6 at time $=300$, and P_d is the corresponding value for the solid line. For local and global noise, the total probability of error P_e is displayed in Fig. 8; for very low and rather high values of the noise power, P_e is almost one. However, there exists an optimal noise strength for which both P_f and $1-P_d$ nearly vanish, resulting in a sharp minimum of P_e.

V. THEORY

The results of Secs. II–IV touch upon two central properties of kink statistics in a discrete bistable chain, namely,

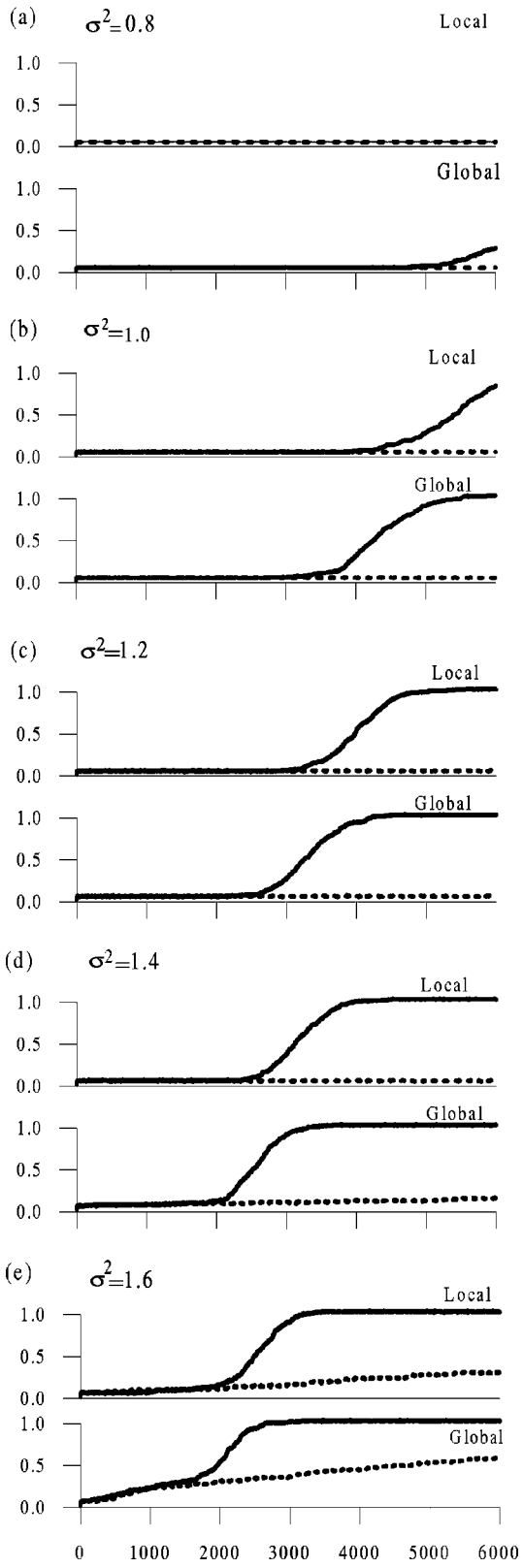

FIG. 6. Arrival probabilities for the discrete model equation (1) with (solid line) and without (dashed curves) an induced kink at site 1, for five local and global noise levels increasing from top to bottom. The propagation distance spans 40 elements. Note that we employ dimensionless units for the noise power σ^2.

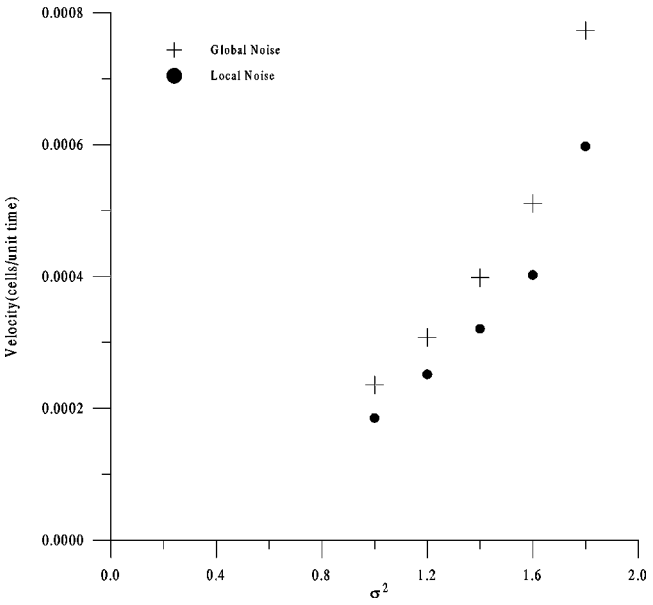

FIG. 7. Numerically measured average kink velocities as a function of noise strength σ^2 (dimensionless) for both global and local noise. It is insightful to compare these values with Fig. 5. As in Fig. 4, the last data point includes a large fraction of spurious kinks, which results in an artificially high value for the velocity.

the Brownian motion of an individual kink and the nucleation of kink-antikink pairs in the presence of an external static bias (or dc forcing term). In the absence of a precise model for the two-state potential that describes the phase shifts in the diode resonators of Sec. II or drives the transmembrane potential of Sec. III, we speculate that the *in situ* bistability of our arrays can be rendered satisfactorily in terms of a double quadratic (DQ) potential, that is by two parabolas displaced by a distance $2a$ [see Fig. 9(a)]. A discrete DQ model is likely to capture, at least qualitatively, the essential features of the array dynamics investigated above, while affording substantial simplifications in its analytical treatment. The analysis of this section can be carried over, with more mathematical effort, to the ϕ^4 model of Sec. III, as well.

The DQ model has been studied both in the continuum [11] and in the discrete case [13]. In dimensionless units the DQ Hamiltonian reads

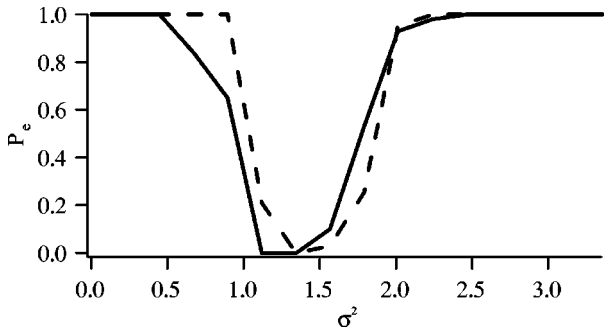

FIG. 8. Total probability of error P_e as a function of noise variance σ^2 (dimensionless) for global (solid line) and local noise (dashed line). For a range of optimal noise strengths, P_e virtually vanishes. The qualitative behavior is robust to variations in the measurement time, which here is taken to be 300 time units.

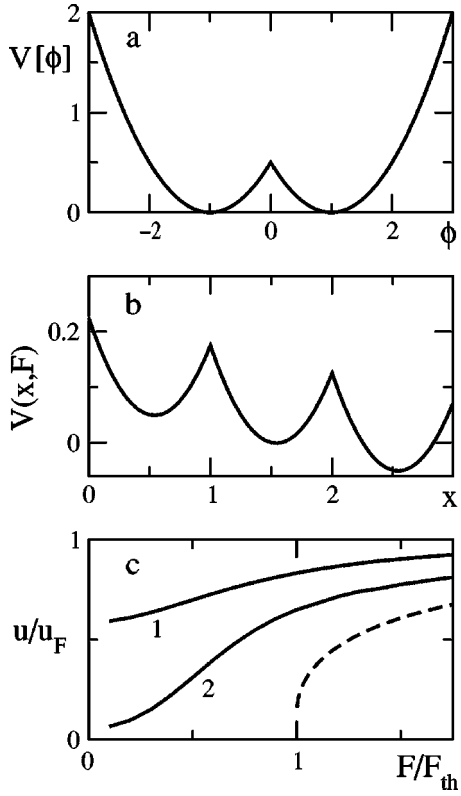

FIG. 9. The double quartic (DQ) model for $\omega_0=c_0=\alpha=1$ and discreteness parameter $\gamma=1$. (a) The DQ potential $V[\phi]$ of Eqs. (4) and (6); (b) The PN potential $V(x,F)$ of Eq. (15) and [18] for $F/F_{th}=0.08$; (c) Kink stationary velocity $u(T)$ versus bias intensity F for $\omega_0^2/kT=20$ (curve 1) and 50 (curve 2). At $T=0+$ the limiting curve (dashed) is given by $u/u_F=0$ for $F<F_{th}$ and $u/u_F=\{(F/F_{th})\ln[F/(F-F_{th})]\}^{-1}$ for $F>F_{th}$. All quantities plotted are dimensionless.

$$\frac{H}{H_0}=l\sum_n\left\{\frac{\dot\phi_n^2}{2}+\frac{c_0^2}{4l^2}[(\phi_n-\phi_{n-1})^2+(\phi_n-\phi_{n+1})^2]+\frac{\omega_0^2}{2}(|\phi|-1)^2\right\}, \tag{4}$$

with $H_0=ma^2/l$. Each ϕ_n can be regarded as the displacement (in units of $2a$) of the nth chain site with mass m, c_0, and ω_0 represent, respectively, the limiting speed and frequency of the phonon modes propagating along the chain and l denotes the chain lattice constant [for instance, in Eq. (1) l was set to 1]. The ratio c_0^2/l^2, which quantifies the effectiveness of the coupling between two adjacent bistable units, is the coupling constant of our model. The importance of the discreteness effects is measured by the *discreteness* parameter

$$\gamma=\frac{c_0^2}{\omega_0 l}\equiv\frac{d}{l}, \tag{5}$$

namely, the ratio of the kink length d to the chain spacing l.

A. Continuum limit

In the continuum (or displacive) limit $\gamma\to\infty$ the Hamiltonian (4) can be expressed as the line integral of the Hamiltonian density

$$H[\phi]=\frac{\phi_t^2}{2}+c_0^2\frac{\phi_x^2}{2}+V[\phi], \tag{6}$$

where the string field $\phi(x,t)$ is defined as $\lim_{l\to0}\phi_{x/l}(t)$ and $V[\phi]=(\omega_0^2/2)(|\phi|-1)^2$. The statistical mechanics of the continuum DQ model can be worked out analytically in great detail [11]. In particular, we know that the kink (ϕ_+) and the antikink solutions (ϕ_-)

$$\phi_\pm(x,t)=\pm\,\mathrm{sgn}[x-X(t)]\left[1-\exp\left(\frac{-|x-X(t)|}{d\sqrt{1-u^2/c_0^2}}\right)^1\right] \tag{7}$$

can be regarded as relativistic quasiparticles with size $d=c_0/\omega_0$, mass $M_0=E_0/c_0^2=1/d$ (or rest energy $E_0=\omega_0 c_0$), and center of mass $X(t)=X_0+ut$.

At low temperatures $kT\ll E_0$, any string configuration can be represented as a linear superposition of randomly distributed kinks and antikinks floating on a phonon bath. A DQ string in equilibrium at temperature T and with boundary conditions $\phi(-\infty,t)=\phi(+\infty,t)$ naturally bears a dilute gas of thermal kink-antikink pairs with density

$$n_0(T)=\frac{1}{2\sqrt{2}}\frac{1}{d}\left(\frac{E_0}{kT}\right)^{1/2}e^{-E_0/kT}. \tag{8}$$

The qualification thermal underscores the fact that n_0 pairs per unit of length (with $n_0 d\ll1$) are being generated by thermal fluctuations alone, irrespective of any geometric constraint at the boundaries (see discussion of Fig. 2 in Sec. II).

B. Kink Brownian motion

The $\phi_\pm(x,t)$ solutions [Eq. (7)] tend to travel with an arbitrary constant speed $u<c_0$, unless perturbed by the coupling to a heat bath or by an external field of force. The simplest heat-bath model was obtained [14] by adding a viscous term $-\alpha\phi_t$ and a zero-mean, Gaussian *local* noise source $\zeta(x,t)$ to the string equation of motion corresponding to the Hamiltonian density (6); that is,

$$\phi_{tt}-c_0^2\phi_{xx}-\omega_0^2\,\mathrm{sgn}[\phi](|\phi|-1)=-\alpha\phi_t+F+\zeta(x,t). \tag{9}$$

Note that all our experiments and simulations have been carried out in the overdamped limit, $\alpha\gg\omega_0$, and in the presence of an additional sub-threshold force F with $F<\omega_0^2$, also incorporated in Eq. (9). Thermalization is imposed here by choosing the noise autocorrelation function $\langle\zeta(x,t)\zeta(x',t')\rangle=2\alpha kT\delta(t-t')\delta(x-x')$.

A single kink (antikink) subjected to thermal fluctuations undergoes driven Brownian motion with Langevin equation

$$\dot X=\mp\frac{2F}{\alpha M_0}+\eta(t), \tag{10}$$

where $\eta(t)$ is a zero-mean-valued Gaussian noise with strength $D=kT/\alpha M_0$ and autocorrelation function $\langle \eta(t)\eta(0)\rangle = 2D\delta(t)$. As apparent from Eq. (10), the external bias pulls $\phi_\pm$ in opposite directions with average speed $\pm u_F$ and $u_F = 2F/\alpha M_0$.

If the local fluctuations are spatially correlated, say

$$\langle \zeta(x,t)\zeta(x',t')\rangle = 2\alpha kT\delta(t-t')[e^{-|x-x'|/\lambda}/2\lambda], \quad (11)$$

the noise strength D changes into [14]

$$D(\lambda) = \frac{Dd}{\lambda+d}\left(1+\frac{\lambda}{\lambda+d}\right). \quad (12)$$

As speculated in Sec. II, for noise correlation length λ smaller than the kink size d possible spatial dishomogeneities become negligible, i.e., $D(\lambda)\simeq D$ for $\lambda \ll d$ [15]. The *global* noise regime simulated both experimentally in Sec. II and numerically in Sec. III corresponds to the limit $\lambda\to\infty$ of the source $\zeta(x,t)$ rescaled by the normalization factor $\sqrt{2\lambda}$; the Langevin equation (10) still applies, but the relevant noise strength is now $\lim_{\lambda\to\infty} 2\lambda D(\lambda) = 4D$. This accounts for the observation that global noise sustains kink propagation more effectively than local noise. Note that the enhancement factor of 4, more exactly $4a$, is nothing but twice the distance of the DQ potential minima (in dimensionless units).

Another important property of global noise is that it cannot trigger the nucleation of a kink-antikink pair and, therefore, minimizes the chances of a ''false alarm'' (see Fig. 3). For this to occur it would be necessary that a spatial deformation of a stable string configuration (vacuum state) be generated large enough for the external bias to succeed in making it grow indefinitely. Such a two-body nucleation mechanism would require a *local* breach of the $\phi\to-\phi$ symmetry of the DQ equation (9), which can be best afforded in the presence of uncorrelated *in situ* fluctuations [16].

The nucleation rate, namely, the number of kink-antikink pairs generated per unit of time and unit of length, can be easily computed by combining the nucleation theory of Ref. [16] with the analytical results of Ref. [11] for the DQ theory. For values of the string parameters relevant to Secs. II–IV—that is, for kT and $Fd \ll E_0$—the stationary DQ nucleation rate can be approximated by [16]

$$\Gamma_1(T) = \frac{2n_0(T)}{\tau(T)} = 2u_F n_0^2(T), \quad (13)$$

if $Fd \ll kT$, or $\Gamma_2(T) = \frac{1}{2}\sqrt{kT/Fd}\,\Gamma_1(T)$, if $kT \ll Fd \ll E_0$ [12]. For an overdamped string, $\alpha \gg \omega_0$ the time constant $\tau(T)$ amounts to the kink (antikink) lifetime prior to a destructive collision with an antikink (kink). Both estimates for the DQ nucleation rate clearly show that spontaneous nucleation of thermal pairs may appreciably degrade local-noise-sustained propagation of injected (or geometric) kinks only for thermal energy fluctuations of the order of the kink rest energy.

C. Peierls-Nabarro potential

Let us go back now to the case of a discrete DQ chain. Discreteness (with parameter γ) affects the kink dynamics on two accounts.

(i) The profile of a *static* kink (antikink) $\phi_\pm(x,0)$ is deformed into [13]

$$\phi^{(s)}_{\pm,n} = \pm\,\mathrm{sgn}[n-N][1-Z_\nu \nu^{|n-N|}], \quad (14)$$

with $Z_\nu = 2\sqrt{\nu}/1+\nu$, $N = m+1/2$, $m = 0, \pm1, \pm2, \ldots$, and $\nu = [\sqrt{1+4\gamma^2}-1]/[\sqrt{1+4\gamma^2}+1]$. To make contact with the displacive solution $\phi_\pm(x,0)$ one must replace nl with x and Nl with X_0, and take the continuum limit $\gamma\to\infty$ (so that $\nu\simeq 1-1/\gamma$). Note that the spatial extension of the discrete kink solutions $\phi^{(s)}_{\pm,n}$ increases monotonically with γ. As γ decreases below unity, $\phi^{(s)}_{\pm,n}$ approaches a step function (order-disorder limit);

(ii) $\phi^{(s)}_{\pm,n}$ is centered midway between two chain sites due to the confining action of an effective [or Peierls-Nabarro (PN)] potential [13]. The PN potential describes the spatial modulation of the $\phi^{(s)}_{\pm,n}$ rest energy as its center of mass is moved across one chain unit cell, say from ml up to $(m+1)l$.

As a result, according to the Langevin equation approach of Sec. V B, the $\phi^{(s)}_{\pm,n}$ center of mass $X(t)$ diffuses on a periodic, piecewise harmonic potential with constant l and angular frequency ω_{PN}, that is [13]

$$\alpha\dot{X} = -\omega_{PN}^2[X - l(\mathrm{int}[X/l]-1/2)] \mp 2F/M_0 + \alpha\eta(t), \quad (15)$$

where $\omega_{PN}^2 \simeq (1+\nu)\omega_0^2$ and $\mathrm{int}[X/l]$ denotes the integer part of X in units of l. Note that $\omega_{PN}\to\omega_0$ and $\omega_{PN}\to\sqrt{2}\,\omega_0$ in the highly discrete and continuum limit, respectively. The energy barriers of the PN potential are thus (almost) quadratic in l.

The one-dimensional Langevin equation (15) has been studied in great detail by Risken [17]. In the noiseless limit $\eta(t)\equiv 0$, the process $X(t)$ is to be found either in a locked state with $\langle\dot{X}\rangle = 0$, for $4F/M_0 < \omega_{PN}^2$, or in a running state with $\langle\dot{X}\rangle \simeq u_F$, for $4F/M_0 > \omega_{PN}^2$. This is indeed the depinning (or locked-to-running) transition described in Fig. 2. At *finite* temperature the stationary velocity $\langle\dot{X}\rangle = u(T)$ can be cast in the form following

$$\frac{u(T)}{u_F} = \frac{1}{\delta}\frac{1-e^{-\delta}}{A-B(1-e^{-\delta})}, \quad (16)$$

where $\delta = 2Fl/kT$ and the quantities A and B can be computed numerically with minimum effort [18]. The ratio $u(T)/u_F$ is the rescaled $\phi^{(s)}_{\pm,n}$ mobility; it crosses from 0 (locked state) over to 1 (running state) continuously in a relatively narrow neighborhood of the threshold value $F_{th} = M_0\omega_{PN}^2/4$. Moreover, $u(T)/u_F$ increases monotonically with T at fixed bias. Such a temperature dependence of the kink mobility explains the sequences of rise curves in Figs. 3 and 6, where kink propagation seems to speed up on raising the noise level.

VI. SUMMARY

In conclusion, the present analysis confirms our speculation that the apparent SR behavior of the efficiency of noise-sustained transmission of kinklike signals along a bistable chain results from two competing mechanisms, both controlled by noise: The driven diffusion dynamics of stable noninteracting kinks, which increases exponentially with the temperature in the vicinity of the depinning transition (propulsion mechanism); The detection of spurious signals, as thermal kink-antikink pairs nucleate with exponentially increasing rates, thus corrupting the propagated signal (garbling mechanism).

If the spatial distribution of the noise was constrained to a small neighborhood around the kink and zero along the rest of the chain, fast and efficient noise supported signal transmission without false alarms would be realizable. This seemingly artificially constructed scenario can be achieved naturally by considering the case of purely multiplicative noise [19]. A detailed study of noise sustained propagation in the presence of multiplicative fluctuations is beyond the scope of this work.

During the preparation of this manuscript the authors learned about recent results on propagation failure in the context of cell differentiation [20]. Utilizing a highly simplified model composed of coupled bistable elements, the authors furnish evidence for the discrete nature of chemical signaling waves propagating through a chain of cells. We speculate that fluctuations, inherent in biological systems, might play a significant role in the details of cell differentiation processes.

ACKNOWLEDGMENTS

We acknowledge the Office of Naval Research for financial support. M.L., N.C., and E.H. warmly thank D. Cigna for very significant contributions to the experimental setup.

[1] SR was introduced by R. Benzi, A. Sutera, and A. Vulpiani, J. Phys. A **14**, L453 (1981); C. Nicolis and G. Nicolis, Tellus **33**, 225 (1981). For reviews, see K. Wiesenfeld and F. Moss, Nature (London) **373**, 33 (1995); A. Bulsara and L. Gammaitoni, Phys. Today **49(3)**, 39 (1996); L. Gammaitoni, P. Hänggi, P. Jung, and F. Marchesoni, Rev. Mod. Phys. **70**, 223 (1998).

[2] R. Benzi, A. Sutera, and A. Vulpiani, J. Phys. A **18**, 2239 (1985); P. Jung, U. Behn, E. Pantazelou, and F. Moss, Phys. Rev. A **46**, R1709 (1991); A. Bulsara and G. Schmera, Phys. Rev. E **47**, 3734 (1993); M. Inchiosa and A. Bulsara, Phys. Lett. A **200**, 283 (1995); J. J. Collins, C. C. Chow, and T. T. Imhoff, Nature (London) **376**, 236 (1995); J. F. Lindner, B. K. Meadows, W. L. Ditto, M. E. Inchiosa, and A. R. Bulsara, Phys. Rev. Lett. **75**, 3 (1995); F. Marchesoni, L. Gammaitoni, and A. R. Bulsara, *ibid.* **76**, 2609 (1996).

[3] P. Jung and G. Mayer-Kress, Phys. Rev. Lett. **74**, 2130 (1995); S. Kádár, J. Wang, and K. Showalter, Nature (London) **391**, 770 (1998); J. F. Lindner, S. Chandramouli, A. R. Bulsara, M. Löcher, and W. L. Ditto, Phys. Rev. Lett. **81**, 5048 (1998).

[4] M. Löcher, D. Cigna, and E. R. Hunt, Phys. Rev. Lett. **80**, 5212 (1998); M. Löcher, D. Cigna, and E. R. Hunt, in *Nonlinear Dynamics: Integrability and Chaos* (Narosa, New Delhi, 1999).

[5] P. Jung, A. Cornell-Bell, K. S. Madden, and F. Moss, J. Neurophysiol. **79**, 1098 (1998); J. Wang, S. Kádár, P. Jung, and K. Showalter, Phys. Rev. Lett. **82**, 855 (1999).

[6] J. P. Keener, J. Theor. Biol. **148**, 49 (1991).

[7] W. C. Cole, J. B. Picone, and N. Sperelakis, Biophys. J. **53**, 809 (1988).

[8] Of course, this is also an approximation. In future work we will replace the discrete cable theory with the *modified cable theory* [6], which incorporates both the discretizing nature of the gap junctions as well as the continuous propagation within a cell.

[9] T. C. Gard, *Introduction to Stochastic Differential Equations* (Decker, New York, 1988).

[10] See, for example, R. N. McDonough and A. D. Whalen, *Detection of Signals in Noise* (Academic Press, New York, 1995).

[11] J. F. Currie, J. A. Krumhansl, A. R. Bishop, and S. E. Trullinger, Phys. Rev. B **22**, 477 (1980).

[12] Fd is essentially the work done by moving the kink through a distance of the order of its radius d. The inequality $Fd \gg kT$ identifies the kink as a pointlike object in comparison with thermal fluctuations.

[13] P. Tchofo Dinda, R. Boesch, E. Coquet, and C. R. Willis, Phys. Rev. B **46**, 3311 (1992).

[14] F. Marchesoni, Phys. Lett. A **115**, 29 (1986); Phys. Rev. Lett. **73**, 2394 (1994).

[15] Diffusion of kinks in a random landscape (like the quenched noise due to resonator array dishomogeneities) has been studied, e.g., by F. Marchesoni, Europhys. Lett. **8**, 83 (1989), by adding a random potential force term to the Langevin equations (10) and (15). For variances of the random potential smaller than the energy fluctuations kT, as in the present investigation, the overall picture of kink dynamics does not change (the diffusion parameters, though, must be rescaled to account for spatial disorder). In the opposite limit and for $\alpha \gg \omega_0$, disorder may provide more efficient a kink pinning mechanism than discreteness.

[16] F. Marchesoni, C. Cattuto, and G. Costantini, Phys. Rev. B **57**, 7930 (1998).

[17] H. Risken, *The Fokker-Planck Equation* (Springer, Berlin, 1984).

[18] The derivation of the (exact) expression Eq. (16) follows Chapter 11 in *The Fokker-Planck Equation* (Ref. [17]). The quantities A and B are defined as follows: $A=\int_0^l e^{-V(x,F)/kT}dx \int_0^l e^{V(x',F)/kT}dx'$ and $B=\int_0^l e^{-V(x,F)/kT}dx \int_0^x e^{V(x',F)/kT}dx'$, with $V(x,F)$ denoting the tilted PN potential $\frac{1}{2}M_0\omega_{PN}^2(x-l/2)^2-2Fx$.

[19] See, for example, P. Tchofo Dinda, Phys. Rev. B **46**, 12 012 (1992); Yu. S. Kivshar and B. A. Malomed, Rev. Mod. Phys. **61**, 763 (1989).

[20] G. Fáth and Z. Domanski, Phys. Rev. E **60**, 4604 (1999).